*Journal of Thermal Analysis and Calorimetry, Vol. 78 (2004) 399–414*

# TG-FTIR STUDY OF GASEOUS COMPOUNDS EVOLVED AT THERMOOXIDATION OF OIL SHALE

*T. Kaljuvee*[1*], *J. Pelt*[2] *and M. Radin*[1]

[1]Department of Chemical and Material Engineering, Tallinn University of Technology, Ehitajate tee 5, 19086 Tallinn, Estonia
[2]Tartu Observatory, 61602 Tõravere, Estonia

## Abstract

The combined thermogravimetric (TG) Fourier transform infrared (FTIR) techniques were used for studying the gaseous compounds evolved at thermooxidation of oil shale samples from different deposits (Estonia, Jordan, Israel). In addition to $H_2O$ and $CO_2$ as the major species, the formation and emission of CO, $SO_2$, HCl and a number of organic species as methane, ethane, ethylene, methanol, formic acid, formaldehyde, chlorobenzene, etc. was determined. Differences in the absorbance of respective bands in FTIR spectra depending on the origin of oil shale and on the heating rate used were established.

**Keywords:** kerogen, oil shale, TG-FTIR, thermooxidation

## Introduction

Thermogravimetric analysis is a suitable method for predicting behaviour of fuels at their thermal processing [1–5], but its potential for identification of gaseous compounds emitted at that is limited. The use of Fourier transform infrared spectroscopy (FTIR) in combination with thermogravimetry (TG) enables to determine simple gaseous compounds as $CO_2$, CO, $H_2O$, etc., as well as different organic compounds formed and emitted during thermal treatment of fuels [6–9].

Estonian oil shale (EOS) is the most important natural resource in Estonia – 90% of energy production in Estonia is based on burning oil shale and the other part (approximately 1.2 million tons yearly) is used in the production of shale oil. The thermal behaviour of Estonian oil shale has been studied considering different aspects of its usage. Several papers are dedicated to the problem of thermal destruction of organic matter (kerogen) [10–12], others to the specific problems of burning oil shale in power plants [13–15]. But only in few works the destruction of Estonian oil shale in an oxidative atmosphere with an attempt to determine gaseous compounds evolved at that has been studied [16–19].

* Author for correspondence: E-mail: gavrich@igic.ras.ru

*1388–6150/2004/ $ 20.00*

*Akadémiai Kiadó, Budapest*
*Kluwer Academic Publishers, Dordrecht*

The aim of this research was thermal characterisation of oil shale samples from different deposits and identification of gaseous compounds formed and emitted at thermooxidation.

## Experimental

*Materials*

Two samples of EOS, one sample of Jordanian (JOS) and Israeli oil shale (IOS) and one sample of Estonian oil shale derivative – SC, the solid remainder formed in the production of shale oil at thermal processing of EOS were studied. The samples were prepared according to ASTM standard D2013-03.

Using different methods of chemical analyses, the chemical composition of these samples was determined as well as their gross calorific (high heating) value (calorimeter B-08BM) and presented in Table 1. For element analyses (Vario EL analyser) the previously air-dried and ground samples were supplementary dried at 105°C for 24 h.

The content of organic matter (kerogen) in the dry samples was calculated as:

$$[100–A^{d}–(CO_2)^{d}_{M}], \%$$

where $A^{d}$ is the content of ash, %; $(CO_2)^{d}_{M}$ is the content of mineral carbon dioxide, %, in dry sample.

**Table 1** Main characteristics of the samples (on dry bases)

| Sample | EOS I | EOS II | JOS | IOS | SC |
|---|---|---|---|---|---|
| Content/% | | | | | |
| Organic matter | 29.7 | 63.1 | 22.6 | 17.1 | 13.1 |
| $(CO_2)_M$ | 19.8 | 5.80 | 15.5 | 22.6 | 18.1 |
| Ash | 50.5 | 32.1 | 61.9 | 60.3 | 68.8 |
| C | 28.3 | 48.5 | 22.2 | 17.1 | 17.9 |
| H | 3.00 | 5.96 | 2.24 | 1.46 | 1.21 |
| N | 0.53 | 0.09 | 0.42 | 0.39 | 0.52 |
| $S_{total}$ | 1.63 | 1.22 | 3.52 | 2.60 | 2.38 |
| $S_{pyr}$ | 1.20 | 0.47 | 0.28 | 0.88 | 0.60 |
| $S_{sulph}$ | 0.10 | 0.04 | 0.12 | 0.32 | 0.44 |
| $S_{sulphide}$ | 0 | 0 | 0 | 0 | 0.60 |
| $S_{org}$ | 0.33 | 0.71 | 3.12 | 1.40 | 0.74 |
| Gross calorific value/ MJ $kg^{-1}$ | 10.24 | 22.43 | 8.14 | 4.90 | 4.12 |

*Methods*

The TG-FTIR system consisted of Setaram Labsys 2000 equipment interfaced to an Interspec 2020 Fourier Transform Infrared Spectrometer. A teflon tube was placed inside the transfer line. The Ranger-AlP Gas Cell, S/N 23790, (REFLEX Analytical Co.) with 8.8 m path length and KBr windows were used. Both, the transfer line and the gas cell were heated to 150°C to prevent condensation. The gas cell was equipped with DTSG (deuterated triglycine sulphate) detector cooled with liquid nitrogen. FTIR measurements were recorded in the 4000–600 $cm^{-1}$ region with a resolution of 4 $cm^{-1}$ and 4 scan average. The Bio-Rad (Sadtler) KnowItAll search program and Gases&Vapours Database (code GS) and Organics&Polymers Database (code TU, SR) were used.

The experiments were carried out under dynamic heating conditions up to 900°C at heating rates of 10 or 50 K $min^{-1}$ in a stream of dry air (70 mL $min^{-1}$). First temperature rate is quite commonly used in thermal analysis, second one is more close to the real temperature conditions in operating boilers, especially in CFB ones. In the case of using the heating rate 50°C $min^{-1}$, the final temperature was held constant during 15 min. Setaram Labsys 2000 enabled simultaneous fixation of TG, DTG and DTA data. Standard 100 μL Pt-crucibles were used; the mass of samples was 20–30 mg.

## Results and discussion

*Thermal analyses*

Essential differences in the thermal behaviour of fuels studied, depending on the origin of fuel and heating rate of samples were observed (Table 2, Figs 1–4). At the heating rate of 10°C $min^{-1}$ thermooxidation proceeded in three steps (not including the emission of absorbed water). The last one proceeded up to 150–180°C and the mass loss at that was in the range of 0.9–2.5%.

The decomposition of kerogen could be roughly divided into two parts. Firstly, decomposition of lighter (more volatile) part of kerogen and, secondly, decomposition of heavier part of kerogen and burning of carbon take place. Depending on the origin of the sample, the first step of thermooxidation of kerogen lasted up to 375–450°C, the second step up to 520–565°C and for EOS II, being very rich in kerogen, even up to 685°C (Figs 1–3, Table 2). However, the boundary between the first and second step of thermooxidation of kerogen could not be clearly defined. These results are quite similar to those presented in [20, 21]. The thermooxidation of pyrite (Table 1) takes place also at higher temperatures. The mass loss during the first step was in between 4.7–19.5%, being the lowest for SC and definitely the highest for EOS II. The mass loss during the second step remained in between 9.0% (IOS) and 42.5% (EOS II) (Table 2). Peaks in DTG curve of EOS I at 362, 388, 508 and shoulders at 318, 338, 443 and 492°C (Fig. 2a) as well as peaks in DTG curve of JOS at 348, 389 and 478°C and shoulders at 294, 453 and 493°C (Fig. 3a) demonstrate well the complexity of decomposition of kerogen. Actually, the chemical composition of kerogen in EOS is extremely complicated [22].

**Table 2** Mass losses and peaks at DTG and DTA curves for the samples

| Sample | Mass loss up to 180°C/% | Temp. range/°C | Mass loss/% | DTG/DTA peak/°C | Temp. range/°C | Mass loss/% | DTG/DTA peak/°C |
|---|---|---|---|---|---|---|---|
| | | | | 10°C $min^{-1}$ | | | |
| EOS I | 0.9 | 180–413 | 13.7 | 362/368<br>388 | 413–565 | 19.7 | 508/513 |
| EOS II | 1.1 | 180–450 | 19.5 | 280/<br>345/346<br>424/402 | 450–685 | 42.5 | 503/550 |
| JOS | 1.5 | 180–380 | 8.0 | 338/33/ | 380–565 | 16.8 | 467/489 |
| IOS | 2.0 | 180–378 | 7.8 | 326/331 | 378–520 | 9.0 | 388/381<br>453/453 |
| SC | 2.5 | 180–375 | 4.7 | 366/342 | 375–560 | 12.9 | 493/502 |
| | | | | 50°C $min^{-1}$ | | | |
| EOS I | 0.7 | 180–494 | 13.1 | 447/371<br>/405<br>/429 | | | |
| EOS II | 0.8 | 180–530 | 38.6 | 454/342 | | | |
| JOS | 0.6 | 180–480 | 10.5 | /400<br>436/438<br>/463 | | | |
| IOS | 0.4 | 180–489 | 7.8 | 328/388<br>/455 | | | |
| SC | 1.1 | 180–486 | 4.6 | 447/451 | | | |

**Table 2** Continued

| Sample | Temperature range/°C | Mass loss/% | DTG/DTA peak/°C | Ash/% |
|---|---|---|---|---|
| | | 10°C min$^{-1}$ | | |
| EOS I | 565–815 | 23.1 | 803/803 | 42.6 |
| EOS I | 685–759 | 5.4 | 736/742 | 31.5 |
| JOS | 565–845 | 15.9 | 787/794 | 57.5 |
| IOS | 520–815 | 23.6 | 800/806 | 57.6 |
| SC | 560–800 | 13.8 | 772/779 | 66.1 |
| | | 50°C min$^{-1}$ | | |
| EOS I | 494–900 | 34.0 | /596<br>/861 | 52.2 |
| EOS II | 530–900 | 24.6 | /518<br>/615<br>/826 | 36.0 |
| JOS | 480–900 | 25.5 | /578<br>/870 | 63.4 |
| IOS | 489–900 | 28.6 | /585<br>/874 | 63.2 |
| SC | 486–900 | 23.4 | /554<br>/867 | 70.9 |

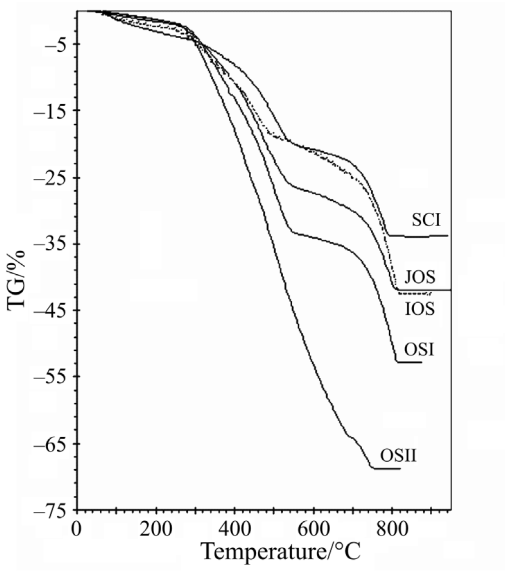


**Fig. 1** TG curves of the samples thermooxidated at a heating rate of 10°C min$^{-1}$

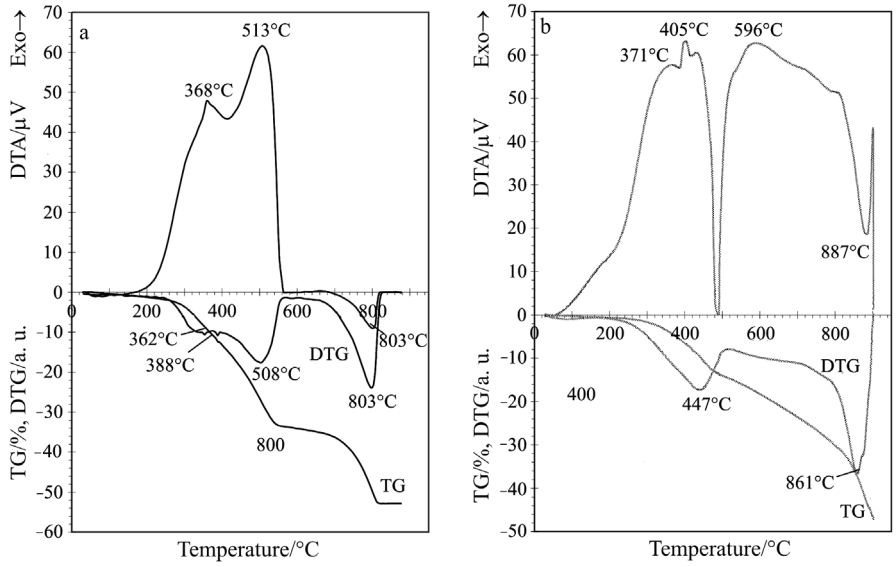


**Fig. 2** Thermoanalytical curves of EOS I at heating rate of a – 10°C min$^{-1}$ and b – 50°C min$^{-1}$

The third step of thermooxidation of the samples is related mainly to the decomposition of carbonates which can be followed by the endoeffect with minimum at 803°C in DTA and DTG curves in Fig. 2a and at 798 and 793°C in Fig. 3a. The

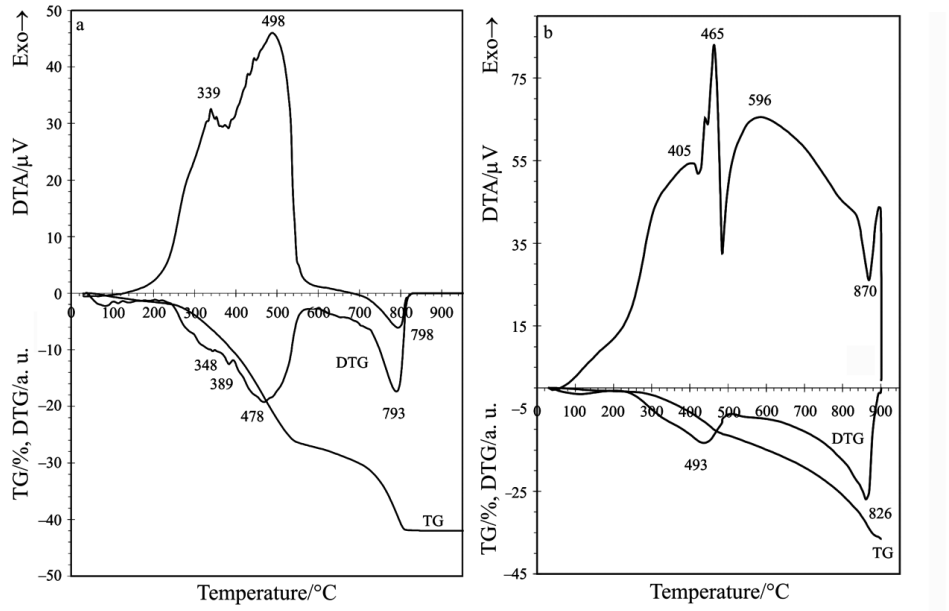


**Fig. 3** Thermoanalytical curves of JOS at heating rate of a – 10°C min$^{-1}$ and b – 50°C min$^{-1}$

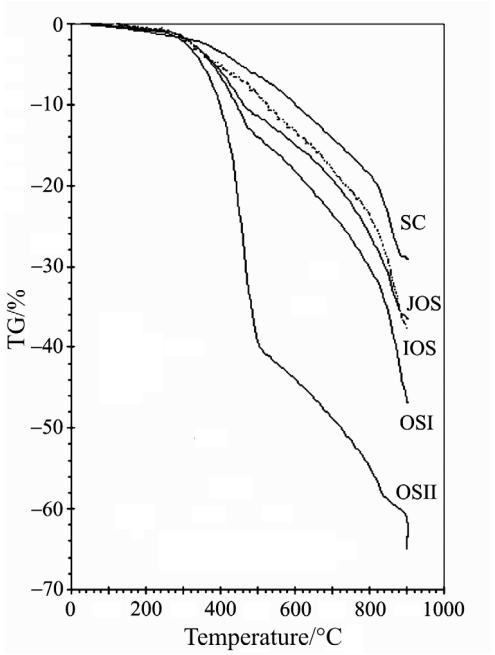


**Fig. 4** TG curves of the samples thermooxidated at a heating rate of 50°C min$^{-1}$

mass loss was completed at 760–815°C and the total mass loss at that varied between 33.9% (SC) and 68.5% (EOS II).

At the heating rate of 50°C $min^{-1}$ the first and the second step of thermooxidation was better differentiated for the samples in which kerogen contains more volatile compounds (estimated by higher content of hydrogen) – Estonian and Jordanian OS samples (Table 1). Yet it was not impossible to differentiate the second and the third step resulting from the incomplete thermooxidation of the heavier part of kerogen before beginning of the decomposition of carbonates at higher heating rate. The peak maxima in DTA and DTG curves as well as the boundary between the first and second step were shifted 50–90°C towards higher temperatures compared to that at low heating speed (Figs 2 and 3) being at that in a good correlation with the results obtained in [23]. The mass loss was hardly completed at 900°C and for EOS I and EOS II samples, respectively, even after 1.5 and 13 min holding at this temperature (Fig. 4). The total mass loss at that was in between 29.1 and 64.0%, being 4–5% smaller than at a low heating rate (Table 2, Figs 1–4). Probably, free Ca, Mg-oxides formed during the decomposition of carbonates took part in the binding of some gaseous compounds, for example, sulphur dioxide [24] and hydrogen chloride [25] into the solid phase.

*FTIR analyses*

In Figs 5–9 the FTIR spectra of gaseous compounds evolved at different temperatures during the TG scan at 10°C $min^{-1}$ heating rate are presented. The two major gaseous compounds evolved at thermooxidation of OS and SC samples studied were $H_2O$ and

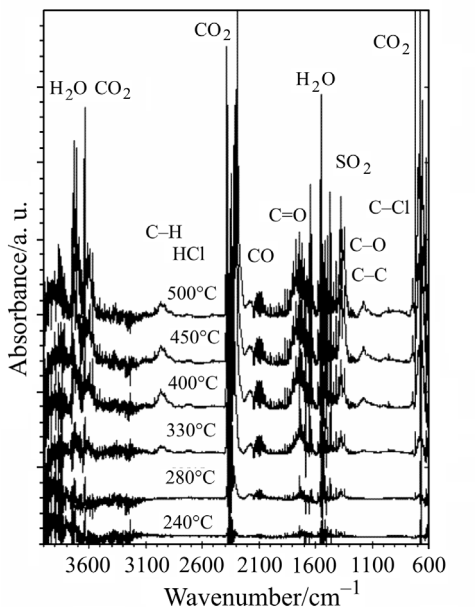


**Fig. 5** FTIR spectra of gaseous compounds evolved at thermooxidation of EOS I at a heating rate of 10°C $min^{-1}$

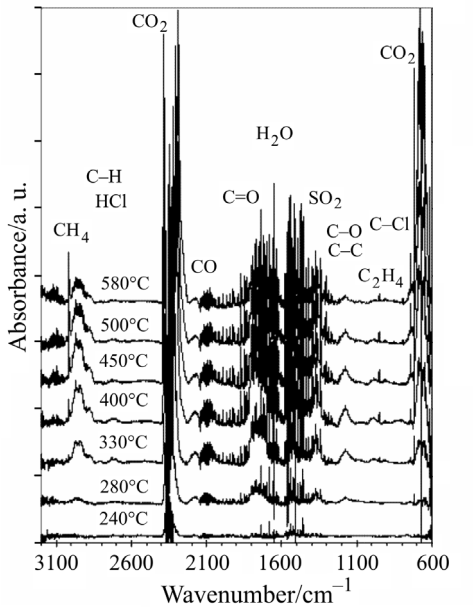


**Fig. 6** FTIR spectra of gaseous compounds evolved at thermooxidation of EOSII (10°C min$^{-1}$)

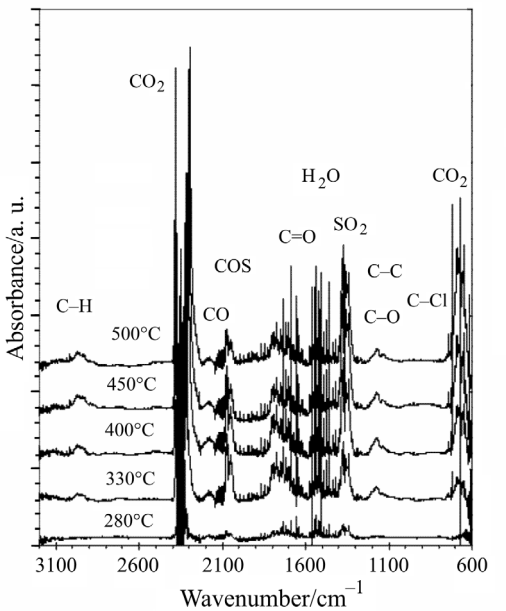


**Fig. 7** FTIR spectra of gaseous compounds evolved at thermooxidation of JOS (10°C min$^{-1}$)

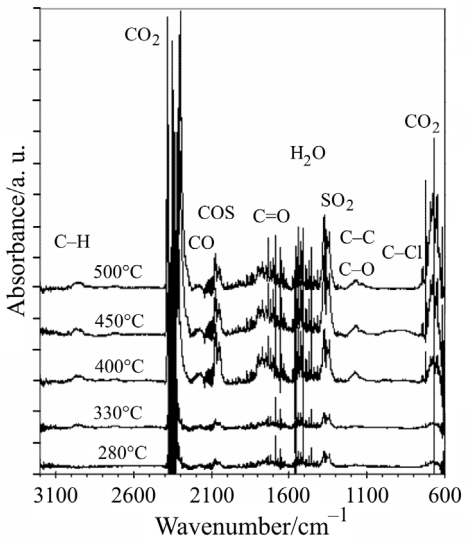


**Fig. 8** FTIR spectra of gaseous compounds evolved at thermooxidation of IOS (10°C $min^{-1}$)

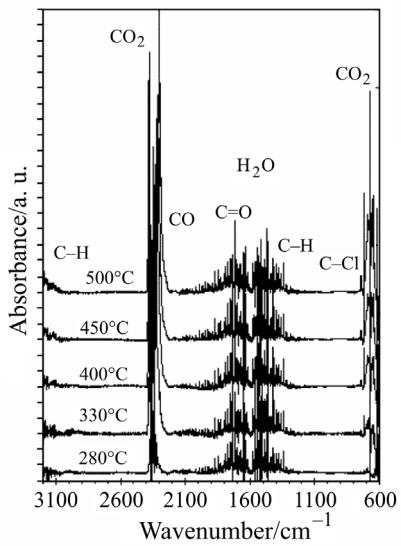


**Fig. 9** FTIR spectra of gaseous compounds evolved at thermooxidation of SC (10°C $min^{-1}$)

$CO_2$. The characteristic water bands in FTIR spectra in broad ranges 3900–3500 and 1900–1300 $cm^{-1}$ indicated that below 180–200°C the only compound evolved was water absorbed in the samples. Actually, the presence of water absorption bands in these ranges makes it more difficult to identify many other gaseous species having their characteristic absorption bands in the same ranges as water. Characteristic peaks for $CO_2$

(2380 and 678 $cm^{-1}$) and CO (2177 and 2114 $cm^{-1}$) appeared at 220–240°C and had maximum absorbance at 500–550 and 350–400°C, respectively.

The appearance of broad bands in FTIR spectra at 3050–2650, at 1800–1650 and at 1300–1000 $cm^{-1}$ caused by C–H, C=O and C–O (C–C) stretching vibrations, respectively, and characteristic bands for C–H bending vibration in $CH_3$ and $CH_2$ groups at 1340–1480 $cm^{-1}$ indicated the beginning of formation and emission of different organic compounds at 260–280°C. The characteristic peaks for methane (3018 and 1307 $cm^{-1}$), ethane (2970 and 1457 $cm^{-1}$), acetic (1798 and 1177 $cm^{-1}$) and formic (1749 and 1107 $cm^{-1}$) acids, formaldehyde (1749 and 1706 $cm^{-1}$) and acetaldehyde (1763 and 1419 $cm^{-1}$) in FTIR spectra was observed, being the most intensive at 400–450°C.

The formation and emission of primary alcohols is characterized by the appearance of C–OH stretching vibration bands at 1075–1000 $cm^{-1}$ and emission of ketones by C=O stretching vibration band at 1710–1720 $cm^{-1}$. The characteristic peaks for methanol (1060, 1035 and 1008 $cm^{-1}$) and ethanol (1244 and 1052 $cm^{-1}$) were also identified in FTIR spectra having the highest intensities like the absorption band similar to the emission of ketones at 400°C.

The possible emission of a small amount of HCl at thermooxidation of EOS samples could be proved by appearing of characteristic absorption bands at 240–330°C at 3000–2700 $cm^{-1}$ which at higher temperatures disappeared or overlapped with more intensive bands of other compounds evolved. The beginning of emission of $SO_2$ (1376, 1361 and in the range of 1200–1100 $cm^{-1}$) was observed at 280–320°C with the maximum absorbance at 450–500°C. The emission of ethylene could be identified by C=C stretching and C–H deformation peaks at 1650 and 950 $cm^{-1}$, respectively, the first appearance of which in FTIR spectra was fixed at 260–280°C with maximum intensities at 400°C.

The formation and emission of chlorobenzene (1474 and 742 $cm^{-1}$), *p*-xylene (1512 and 793 $cm^{-1}$) and possibly furan (745 $cm^{-1}$) [8] were identified by the appearance of these characteristic peaks in FTIR spectra at 330–400°C with the maximum absorbance at 500–550°C.

Comparing the FTIR spectra of different samples (and especially of these for EOS and its SC having the same origin), the differences were observed in the intensities of respective bands of different gaseous species evolved. In FTIR spectra of OS II (Fig. 6) the bands characteristic to more volatile compounds as methane, ethane, ethylene, but also to methanol, compounds of carbonyl group and even to chlorobenzene were more intensive. In FTIR spectra of SC (Fig. 9) prevailed absorption bands of $CO_2$ and $H_2O$, but these for water were less intensive than the respective bands in FTIR spectra of EOS I. In addition of water the absorption bands characteristic to CO, ethylene, methane, ethane, compounds of carbonyl group, chlorobenzene and *p*-xylene were also less intensive (Fig. 5). $SO_2$ and methanol were fixed on the level of traces. This was in a good correlation with the content of kerogen in these samples and, especially, with the element composition of kerogen – the higher the content of hydrogen in the samples (Table 1) the higher, as a rule, the amount of volatile organic compounds was.

Some principal differences in FTIR spectra were observed comparing of these of EOS (Figs 5 and 6), JOS (Fig. 7) and IOS (Fig. 8). In FTIR spectra of JOS and IOS absorption bands characteristic to COS (2075 and 2053 $cm^{-1}$) and HCN (713 $cm^{-1}$) were observed. This could be explained by the higher content of organic sulphur and organic nitrogen in these samples (Table 1). In FTIR spectra of EOS I, having similar organic nitrogen content, the HCN absorption band was presented only as a weak shoulder near 713 $cm^{-1}$.

For better characterisation of differences in the thermal behaviour of different oil shale and semicoke samples, the absorption bands for ethylene and chlorobenzene were presented more precisely in Figs 10a and b, respectively. The intensities of the absorption band of more volatile compound – ethylene are in a good correlation with the content of kerogen and the content of hydrogen in kerogen in these fuels. The most intensive it was for EOS II and the weakest for IOS. Considering the temperature of maximum intensities of the absorption bands of ethylene (350–400°C) it could be concluded that the formation of ethylene and other volatile species is connected to the decomposition of the lighter (more volatile) part of kerogen. So expressive differences in the intensities of the absorption bands corresponding to chlorobenzene in different fuels were not observed. Considering the temperature of maximum intensities of these bands, the formation of chlorobenzene as well as *p*-xylene and furan is mainly connected to the decomposition of the heavier part of kerogen.

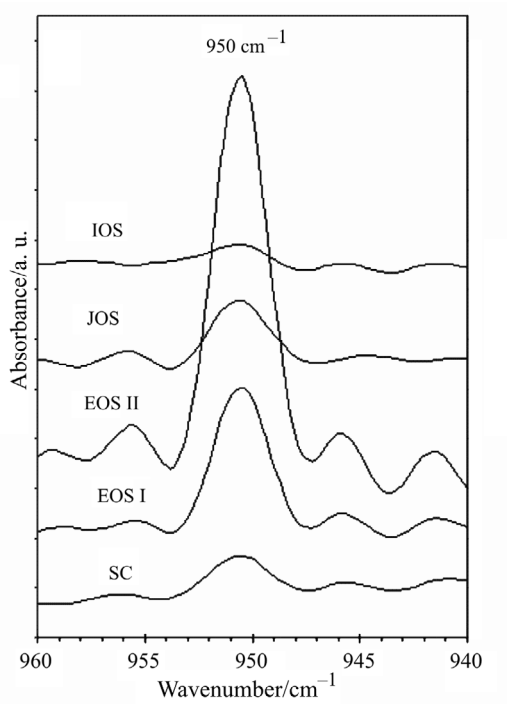


**Fig. 10a** Characteristic peak of ethylene at 950 $cm^{-1}$ for different samples at 400°C (10°C $min^{-1}$)

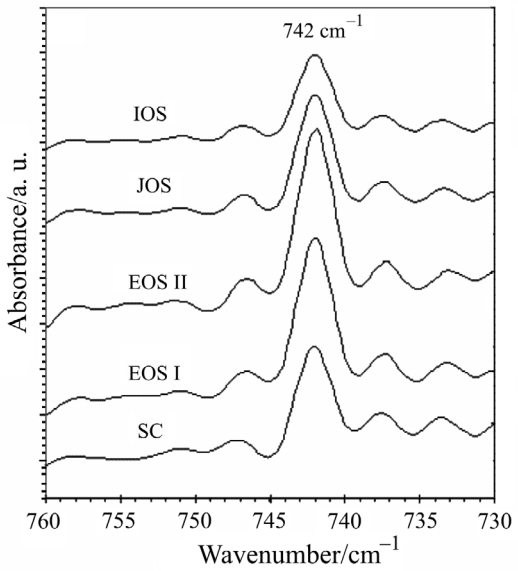


**Fig. 10b** Characteristic peak of chlorobenzene at 742 cm$^{-1}$ for different samples at 500°C (10°C min$^{-1}$)

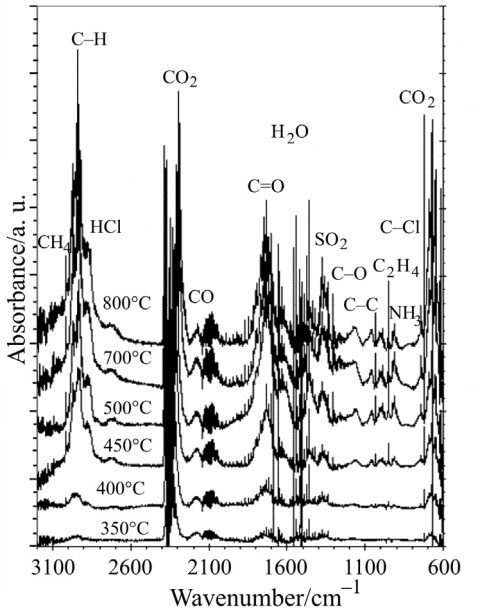


**Fig. 11** FTIR spectra of gaseous compounds evolved at thermooxidation of EOS II at a heating rate of 50°C min$^{-1}$

At fast heating (50°C $min^{-1}$) the beginning of evolution of organic compounds was shifted by 60–80°C towards higher temperatures, absorption bands of respective gaseous species in FTIR spectra (the concentration of respective compounds evolved) were, as a rule, more intensive and the emission of different species at that lasted up to 800–900°C (Figs 11 and 12). So, in addition to methane, ethane and ethylene (Fig. 12a), quite intensive absorption bands in FTIR spectra had also $SO_2$, CO, methanol (Fig. 12b) and compounds of carbonyl group. The differences in the intensities of absorption bands characteristic to chlorobenzene, *p*-xylene and furan were not so expressive as in the case of the above mentioned compounds. It could be explained, firstly, by the worse interaction conditions between solid and gaseous phases as the diffusion of oxygen into the pores of oil shale (kerogen) compared to that at low heating rate is much more hindered due to the higher partial pressure of formed and evolved gaseous species. Secondly, the total amount of organic gaseous species evolved per unite of time is much bigger and, consequently, the contact-time between oxygen and organic gaseous species is not enough to guarantee the complete oxidation of them before leaving the furnace.

One more principal difference was observed – at high heating rate organic nitrogen decomposed preferably with the formation of $NH_3$ (967 and 932 $cm^{-1}$) (Fig. 12a).

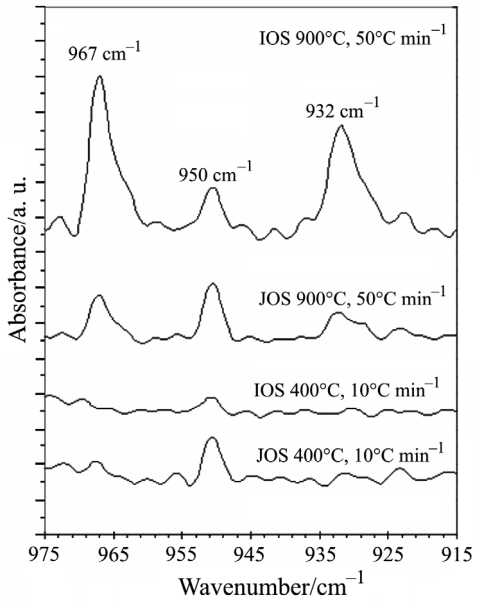


**Fig. 12a** Characteristic peaks of $NH_3$ (967 $cm^{-1}$ and 932 $cm^{-1}$) and ethylene (950 $cm^{-1}$) for JOS and IOS thermooxidated at different heating rate

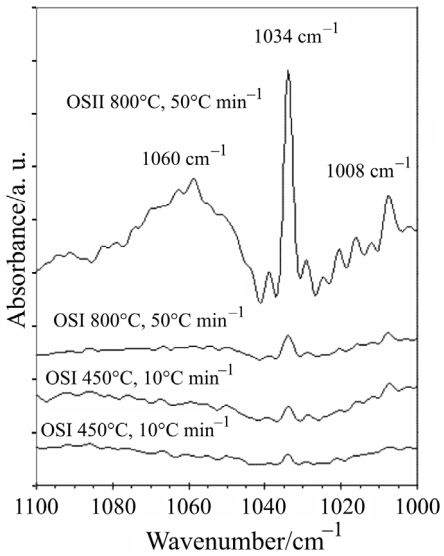


**Fig. 12b** Characteristic peaks of methanol for EOS samples thermooxidated at different heating rate

## Conclusions

The combined TG-FTIR study of thermooxidation of oil shale samples and its semicoke made it possible to determine the differences in the thermal behaviour of different samples and to identify a number of gaseous species formed and evolved at that. The differences in the intensities of the absorption bands of these species in FTIR spectra depending on the chemical composition of the samples and on the heating rate used was observed.

At low heating rate (10°C $min^{-1}$) the formation and emission of $CO_2$, $H_2O$, CO, $SO_2$, methane, ethane, ethylene, methanol, formic acid, formaldehyde, chlorobenzene were clearly identified in FTIR spectra of all the samples studied. The formation of ethanol, acetaldehyde, HCl and possibly furan, at least on the level of traces, were also identified. The most intensive emission of CO took place at 350–400°C, that of ethane, ethylene, acetic and formic acids, formaldehyde and methanol at 400–450°C, of methane and $SO_2$ at 450–500°C, of $CO_2$, chlorobenzene and *p*-xylene at 500–550°C.

Due to the high content of organic sulphur and organic nitrogen in Jordanian and Israeli oil shale samples, also the formation of COS and HCN was observed.

At high heating rate (50°C $min^{-1}$) the beginning of evolution of organic compounds was shifted by 60–80°C towards higher temperatures, the absorption bands of the respective gaseous species in FTIR spectra were, as a rule, more intensive, the emission of different species lasted up to 800–900°C and the organic nitrogen decomposed with the formation of ammonia.

A good correlation between the absorbance of bands characteristic to volatile organic compounds evolved and the elemental composition of the samples (of kerogen) was observed.

* * *

This work was partly supported by Estonian Science Foundation (G5606, G4697).

## References

1 S. Cebulak, A. Gawęda and A. Langier-Kuzniarowa, J. Therm. Anal. Cal., 56 (1999) 917.
2 M. B. Folgueras, R. M. Díaz, J. Xiberta and I. Prieto, Fuel, 82 (2003) 2051.
3 K. E. Benfell, B. B. Beamish and K. A. Rodgers, Thermochim. Acta, 297 (1997) 79.
4 L. B. Méndez, A. G. Borrego, M. R. Martinez-Tarazona and R. Menéndez, Fuel, 82 (2003) 1875.
5 Y. Ninomiya, L. Zhang, T. Sakano, C. Kanaoka and M. Masui, Fuel, 83 (2004) 751.
6 R. M. Carangelo, P. R. Solomon and D. J. Gerson, Fuel, 66 (1987) 960.
7 I. Pitkänen, J. Huttunen, H. Halttunen and R. Vesterinen, J. Therm. Anal. Cal., 56 (1999) 1253.
8 R. Lu, S. Purushotama, X. Yang, J. Hyatt, W.-P. Pan, J. T. Riley and W. G. Lloyd, Fuel Process. Technol., 59 (1999) 35.
9 A. Zanier, J. Therm. Anal. Cal., 56 (1999) 1389.
10 A. Aarna, Oil Shale, 12 (1995) 203.
11 I. Blyakhina and K. Urov, Oil Shale, 10 (1993) 187.
12 V. Yefimov, Oil Shale, 17 (2000) 367.
13 H. Holopainen, Oil Shale, 8 (1991) 194.
14 H. Arro, A. Prikk and J. Kasemetsa, Oil Shale, 14 (1997) 215.
15 H. Arro, A. Prikk and T. Pihu, Fuel, 82 (2003) 2179.
16 H. Kundel and L. Petaja, Oil Shale, 2 (1985) 373 (in Russian).
17 A. Ots, Oil Shale, 9 (1992) 63.
18 M. Koel and K. Urov, Oil Shale, 10 (1993) 261.
19 T. Kaljuvee, R. Kuusik and A. Trikkel, J. Therm. Anal. Cal., 72 (2003) 393.
20 M. V. Kök and M. R. Pamir, J. Anal. Appl. Pyrolysis, 55 (2000) 185.
21 M. V. Kök, Oil Shale, 18 (2001) 131.
22 Ü. Lille, Oil Shale, 19 (2002) 3.
23 M. V. Kök and M. R. Pamir, J. Therm. Anal. Cal., 53 (1998) 567.
24 T. Kaljuvee and R. Kuusik, J. Therm. Anal. Cal., 56 (1999) 1243.
25 K. Liu, W-P. Pan and J. T. Riley, Fuel, 79 (2000) 1115.